Structural evolution and skyrmionic phase diagram of the lacunar spinel GaMo₄Se₈

Emily C. Schueller,¹ Daniil A. Kitchaev,¹ Julia L. Zuo,¹ Joshua D. Bocarsly,¹ Joya A. Cooley,¹ Anton Van der Ven,¹ Stephen D. Wilson,¹ and Ram Seshadri¹

¹Materials Department and Materials Research Laboratory University of California, Santa Barbara, Santa Barbara, CA, 93106 (Dated: March 16, 2020)

In the AB_4Q_8 lacunar spinels, the electronic structure is described on the basis of interand intracluster interactions of tetrahedral B_4 clusters, and tuning these can lead to myriad fascinating electronic and magnetic ground states. In this work, we employ magnetic measurements, synchrotron X-ray and neutron scattering, and first-principles electronic structure calculations to examine the coupling between structural and magnetic phase evolution in ${\rm GaMo_4Se_8}$, including the emergence of a skyrmionic regime in the magnetic phase diagram. We show that the competition between two distinct Jahn-Teller distortions of the room temperature cubic $F\overline{4}3m$ structure leads to the coexistence of the ground state R3m phase and a metastable Imm2 phase. The magnetic properties of these two phases are computationally shown to be very different, with the Imm2 phase exhibiting uniaxial ferromagnetism and the R3m phase hosting a complex magnetic phase diagram including equilibrium Néel-type skyrmions stable from nearly $T=28\,{\rm K}$ down to $T=2\,{\rm K}$, the lowest measured temperature. The large change in magnetic behavior induced by a small structural distortion reveals that ${\rm GaMo_4Se_8}$ is an exciting candidate material for tuning exotic magnetic properties via mechanical means.

I. INTRODUCTION

In recent years, there has been the increasing recognition that in some transition metal compounds, metalmetal bonding can often interact with electron correlation resulting unconventional magnetic and electronic behavior, as well as unusually strong coupling between magnetic, electronic, and structural degrees of freedom [1–4]. An important class of materials where this becomes evident are the lacunar spinels, which are characterized by tetrahedral clusters of transition metal atoms [5]. Two members of the lacunar spinel family, GaV₄S₈ and GaV₄Se₈, have garnered significant attention in recent years as multiferroic materials as well as Néeltype skyrmion hosts [6–8]. At low temperatures, these materials crystallize in the polar R3m space group [9] and support complex magnetic phase diagrams with an ordered moment of $1 \mu_B/V_4$ cluster. The related Mocontaining compounds, GaMo₄S₈ and GaMo₄Se₈, have been less studied, although they are reported to have a similar low temperature crystal structure, but with a compressive rather than elongative distortion along the cubic [111] direction [9-11]. Bulk magnetic measurements have revealed similar metamagnetic behavior between the Mo and the V-containing compounds [12, 13], while computational analysis of lacunar spinel ferromagnets suggests that all materials with this structure type are likely to host skyrmions across wide temperature ranges [14]. However, because Mo is a heavier element than V, the Mo-based compounds exhibit increased spin-orbit coupling, leading to more pronounced magnetic anomalies over greater regions of magnetic field and temperature. Additionally, spin-orbit coupling can affect the electronic properties through splitting of degenerate molecular orbitals, as seen in GaTa₄Se₈ [15]. A recent report on GaMo₄S₈ indicates that this material harbors complex modulated magnetic phases and that the increased spin–orbit coupling in the material leads to unusual "waving" effects on the magnetic ordering vectors [16].

In this work, we perform a detailed theoretical and experimental study of GaMo₄Se₈ in order to characterize the coupling between the crystal structure evolution and magnetic properties. We discover that at the structural phase transition, GaMo₄Se₈ can transform into two polar space groups, the reported rhombohedral R3m phase, which is the ground state, and an orthorhombic Imm2phase, which is metastable. On the basis of computational and experimental data, we show that the R3mphase of GaMo₄Se₈ hosts a rich magnetic phase diagram with long wavelength magnetic order, including cycloids and Néel-type skyrmions, with periodicities on the order of 16 nm. In contrast, the competing Imm2phase is suggested from first-principles calculations to be a strongly uniaxial ferromagnet. The dramatic change in magnetic behavior associated with a subtle change in crystal structure highlights the strong coupling between crystal structure and magnetism in GaMo₄Se₈, and suggests an avenue for tuning skyrmion and other exotic magnetic phases via strain.

II. METHODS

A. Computational Methods

All electronic structure calculations were performed using the Vienna Ab–Initio Simulation Package (VASP) [17] with projector-augmented-wave pseudopotentials [18, 19] within the Perdew–Burke–Ernzerhof generalized gradient approximation [20]. We do not employ an atom-centered Hubbard–U correction as our previous analysis of the related GaV_4Se_8 system showed that this leads to an incorrect high–moment magnetic configura-

tion by penalizing metal-metal bonding [4]. Structural distortions from the high temperature cubic structure to the low temperature orthorhombic and rhombohedral structures were generated using ISODISTORT [21]. Structural stability calculations used a Gamma-centered k-point grid of $8\times8\times8$ and an energy cutoff of 500 eV with a collinear magnetic configuration of $1 \mu_B/\text{Mo}_4$. Computational results were parsed and visualized with the python package pymatgen [22]. Noncollinear magnetic calculations accounting for spin-orbit coupling followed the methodology described by Kitchaev et al. [14]. All calculations were performed statically, on the basis of the experimentally determined crystal structures, and converged to 10^{-6} eV in total energy. To reduce noise associated with ik-point discretization error, all spinconfiguration energies were referenced to the energy of a *c*-axis ferromagnet computed within the same supercell.

The magnetic cluster expansion Hamiltonian [14, 23– 25] used to construct the magnetic phase diagram was derived by considering single-spin and nearest-neighbor pair interactions, as shown in Supplementary Figure S3. The interaction strengths were parametrized on the basis of collinear and spin-wave enumerations up to a supercell size of 4, as well as several sets of spin configurations iteratively generated to independently constrain the terms in the Hamiltonian.[26] Note that due to the very small energy scale of magnetocrystalline anisotropy, we fit the single-site anisotropy coefficients independently of the pair interactions, by fitting to the energy of rotating the ground-state collinear spin configurations within the primitive cell of the structure, so as to eliminate all noise arising from changes in the k-point grid [14]. The resulting parametrization leads to an error below $5 \,\mu\text{eV/Mo}_4$ for the magnetocrystalline anisotropy, and below 1 meV/Mo₄ across all non-collinear spin configurations, as shown in Supplementary Figure S4. The full Hamiltonians and fitted interaction parameters for the R3m and Imm2 phases are given in Supplementary Tables 1 and 2.

B. Experimental Methods

 $GaMo_4Se_8$ powder was obtained by reaction of Ga pieces and ground Mo and Se powders with an approximately 50% excess of elemental Ga. The elements were reacted in an evacuated fused silica tube in 1 g batches with a heating ramp rate of 8° C/min to 1010° C, held for 20 hours, and quenched [27].

High resolution synchrotron powder X-ray diffraction was performed at the Advanced Photon Source at Argonne National Laboratory at the 11-BM beamline. Approximately 30 mg of powder was loaded into a kapton capillary and placed into a cryostat for 30 min. temperature-dependent scans from $T=10\,\mathrm{K}$ to $T=250\,\mathrm{K}$. Rietveld refinements were performed using the Topas analysis package [28]. Low–temperature structure solution was performed by first fitting the re-

ported rhombohedral structure and then indexing the remaining structural peaks using the EXPO2014 software. The symmetry of the unit cell generated by EXPO was compared to various subgroups of the high temperature $F\overline{4}3m$ structure using the ISODISTORT software package [21]. A structure for the corresponding orthorhombic Imm2 space group was generated using ISODISTORT and Rietveld refinements of both the rhombohedral and orthorhombic phases were performed using TOPAS Academic [28]. Due to hkl-dependent strain, the Stephens peak shape was used in conjunction with Gaussian size broadening to fit the highly anisotropic peak shapes. Crystal structures were visualized using the VESTA software suite [29].

Small angle neutron scattering measurements were performed at the National Institute of Standards and Technology (NIST) NG-7 neutron beamline. Approximately 100 mg of powder was cold-pressed into a 5 mm pellet and placed into a cryostat. Exposures were taken over 8 h durations at various applied magnetic fields below the magnetic ordering temperature and a 3 h background scan was performed above the magnetic ordering temperature. The data integration and background subtraction was performed in the IGOR pro software [30].

Bulk magnetic measurements were performed on a Quantum Design MPMS 3 SQUID Vibrating Sample Magnetometer, with approximately 30 mg of powder loaded into a plastic container and mounted in a brass holder. DC magnetization vs. field scans were performed on increasing field and AC susceptibility vs. field measurements were performed on decreasing field. For magnetoentropic mapping measurements, temperature-dependent magnetization measurements from 2 K to 40 K were performed with applied magnetic fields varying from 0 Oe to 4000 Oe in increments of 75 Oe. Derivatives and Δ Sm calculations were performed using python code available from Bocarsly et al. [31].

III. RESULTS

GaMo₄Se₈ is a member of the lacunar family with a cubic noncentrosymmetric crystal structure at room temperature characterized by tetrahedral clusters of Mo atoms, as shown in Figure 1(a). These clusters behave like molecular units with a spin of $1 \mu_B$ per Mo₄ cluster. V-containing members of the lacunar spinel family have been reported to host complex magnetic phase diagrams including cycloids and Néel-type skyrmions [6-8]. Recently, a small angle neutron scattering (SANS) study on a single crystal of GaMo₄S₈ has revealed that it too has exotic low temperature modulated magnetic phases [16], while computational results have suggested that all Mo and V-containing lacunar spinels with a low temperature R3m structure are likely to host skyrmion phases [14]. The origin of this behavior is a structural Jahn–Teller transition which occurs at temperatures below room temperature but above the magnetic ordering

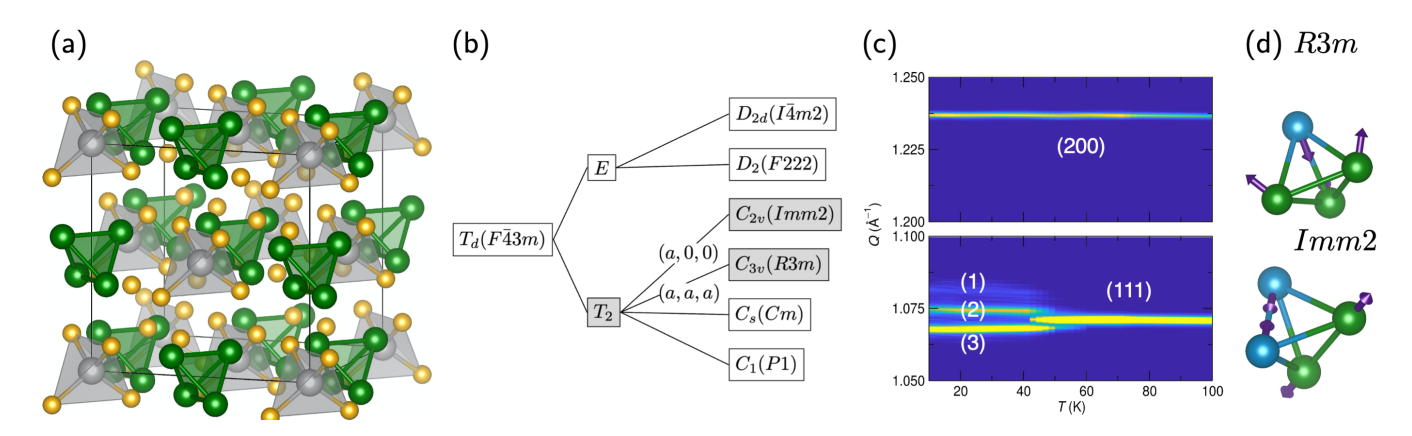


FIG. 1. (a) The cubic F43m crystal structure of $GaMo_4Se_8$, characterized by tetrahedral clusters of Mo atoms. (b) All subgroups of F43m which keep the primitive unit cell volume the same. R3m and Imm2 both follow the T_2 irrep but through different order parameter directions. (c) The evolution of peaks upon cooling in synchrotron XRD data. At 50 K the (111) cubic peak splits into 3 while the (200) cubic peak stays undistorted. Because the middle peak of the (111) split shifts relative to the peak in the cubic phase while the (200) peak does not shift, it is not possible to explain the low temperature structure by a combination of the cubic phase and a single low temperature phase. (d) The distortion of the M_0 4 tetrahedron as it goes into the M_0 4 and M_0 5 are groups. Both are polar, but the M_0 6 cluster has lower symmetry, with three unique bond lengths, compared to two in the M_0 6 cluster.

temperature. This lowers the symmetry of the crystal and thereby relieves the degeneracy of the partially occupied t_2 molecular orbital of the high-temperature $F\overline{4}3m$ structure. In the V– and Mo–containing compounds, the low–temperature ground state has R3m symmetry, which allows for Dzyaloshinskii–Moriya interactions and the emergence of chiral magnetic phases. This structure is also polar, and the coexistence of magnetic and polar order makes $GaMo_4Se_8$ and related compounds multiferroic materials.

We find that ${\rm GaMo_4Se_8}$ follows qualitatively similar behavior to ${\rm GaV_4Se_8}$, with complex magnetic order arising from a Jahn–Teller distortion of the high–temperature $F\overline{4}3m$ structure. However, in addition to the R3m ground state, ${\rm GaMo_4Se_8}$ forms a competing metastable Imm2 phase, defined by an orthorhombic Jahn–Teller distortion and distinctly different magnetic properties. We first characterize the formation and coexistence of these two structures, and then establish how the character of the low–temperature distortion controls the magnetic phase diagram of each phase.

Figure 1(c) shows high-resolution synchrotron powder diffraction data as a function of temperature. At $T=50\,\mathrm{K}$, the (111) cubic peak splits into 3 peaks, with the two outer peaks corresponding to an R3m distortion. Previous X–ray diffraction studies of the structural phase transition of $\mathrm{GaMo_4Se_8}$ have rationalized the presence of extra peaks below the transition temperature ($T=51\,\mathrm{K}$) as the coexistence of the high temperature cubic F43m phase and the rhombohedral R3m phase [10]. However, with high–resolution measurements employed here, we find that the low–temperature data cannot be fit by a combination of the R3m phase and the F43m phase. The middle peak shown in the lower panel of Figure 1(c), which was previously assumed to be a continuation of

the cubic $(F\overline{4}3m)$ phase, shifts significantly at the phase transition, while the higher Q peak [cubic (200)] shown in the top panel does not split or shift at the phase transition. Because there is only one lattice parameter in the cubic phase, it cannot support a shift of one peak but not another, meaning that there must be another explanation for the additional peaks.

We performed a search for a lower symmetry subgroup of R3m (such as a monoclinic C2/m phase) that could explain the additional peaks, but found none that did not add add extraneous peaks, not present in the data. We indexed the peaks that could not be explained by the R3m unit cell and found they corresponded to an orthorhombic, polar Imm2 phase. Imm2, while a subgroup of the parent $F\overline{4}3m$ structure, is not a subgroup of the R3m space group. The transition pathways from the $F\overline{4}3m$ phase to the R3m and Imm2 phases are associated with two different order parameter directions, but with the same irreducible representation (T_2) as shown in Figure 1(c), indicating the two subgroups are symmetrically similar. The difference between the two structures is most obvious in the distortion of the Mo4 tetrahedron through the phase transition, indicated by the arrows in Figure 1(d), which leads to 2 sets of Mo-Mo bond lengths in the R3m phase and 3 sets in the Imm2 phase.

It is clear from the diffraction data that the R3m and Imm2 phases form simultaneously and coexist in the powder. However, the structures are noticeably strained, as evidenced by the broad line shapes, and have a large amount of peak overlap due to their similarity, which introduces uncertainty in the determination of relative weight percentages of the two phases. As seen in Figure 2(a), our best fit to the data at T=,10 K yields about 30% of the orthorhombic phase and 70% of the rhombohedral phase. In order to fit the unusual peak shapes,

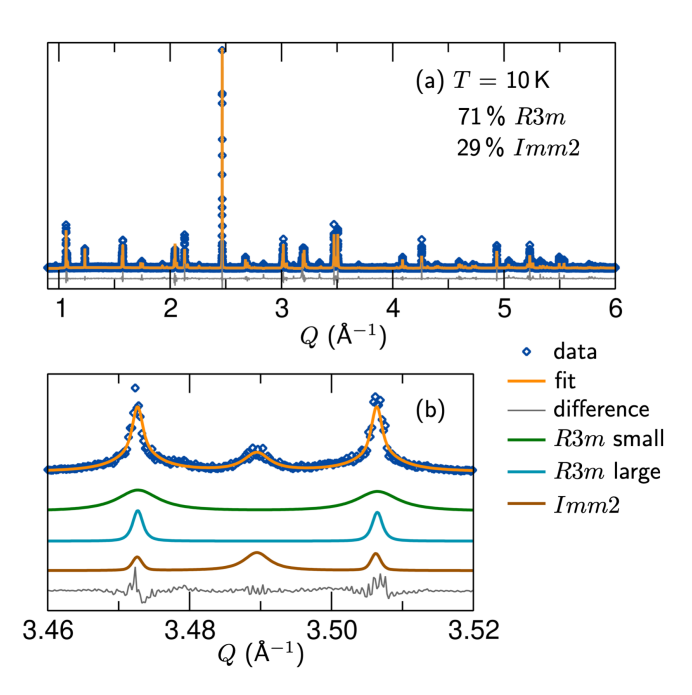


FIG. 2. (a) At 10 K, there is about 70% of the rhombohedral phase and 30% of the orthorhombic phase. (b) The complex peak shapes can be fit with two R3m phases with different particle sizes, and an Imm2 phase with hkl-dependent strain broadening.

we use two phases for the R3m structure, one with small particles (strong effects of size broadening) and one with large particles, both with strain effects. The Imm2 phase is fit with hkl-dependent strain broadening using the Stephens peak-shape. This combination of phases to describe a single peak is shown in Figure 2(b). At $T=50\,\mathrm{K}$, the diffraction data is best fit by a combination of the cubic phase and both the R3m and Imm2 phases, indicating both phases form simultaneously at the phase transition temperature and there is no phase region with only one of the two low temperature structures. A similar phase transition from a high symmetry structure into two subgroups has been reported in the oxide spinels $MgCr_2O_4$ and $ZnCr_2O_4$ and was attributed to internal strain creating a metastable and stable phase [32].

To probe the energy landscape for these two phases, we turn to density functional theory (DFT) calculations. We find that while the R3m phase is the ground state structure, its formation may be kinetically suppressed relative to the Imm2 phase. Using ISODISTORT, we generated distorted structures along the path from the $F\overline{4}3m$ phase to the R3m phase and the Imm2 phase. These calculations show that the orthorhombic structure is less stable than the rhombohedral structure by about $20\,\text{meV/Mo}_4$ cluster, as shown in Figure 3(a). However, the transition pathway leading to the R3m phase has a small energy barrier, while the formation of the Imm2 phase appears to be barrier-less. Furthermore, we observe experimentally that the percentage of the R3m phase increases with decreasing temperature, as can be

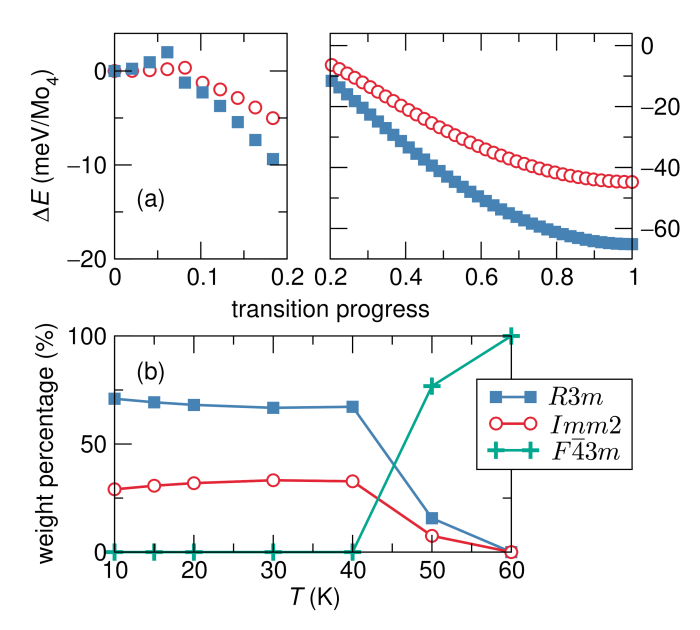


FIG. 3. (a) DFT energies along the transition pathways from the cubic phase to the rhombohedral and orthorhombic phases. The R3m structure has lower energy, making it the ground state structure, but it has a formation energy barrier, highlighted in the left panel. The energy difference is $20\,\mathrm{meV/Mo_4}$ cluster. (b) The phase evolution of $\mathrm{GaMo_4Se_8}$. Upon cooling, the percentage of the R3m phase slightly increases, indicating it is likely the ground state crystal structure.

seen in Figure 3(b). Thus, both computation and experiments indicate that the R3m arrangement is the likely ground state. Nonetheless, it is possible that due to the low temperature of the phase transition ($T=51\,\mathrm{K}$), the material could get trapped in the orthorhombic structure and lack the energy to convert to the rhombohedral structure. It is also likely that strain effects impact the energy landscape of the two phases and could stabilize the Imm2 phase.

A. Magnetic behavior coupled to structural transition

Analogous to other lacunar spinels, the magnetic behavior of GaMo₄Se₈ is closely tied to its crystal structure. Temperature-dependent magnetization data reveals largely ferromagnetic ordering with an ordering temperature of approximately $T = 27.5 \,\mathrm{K}$, in agreement with previous reports [13]. GaMo₄Se₈ has a saturation magnetization of $1 \mu_B/\text{Mo}_4$ cluster, as shown in Figure 4(a), in agreement with literature [13] and molecular orbital theory. However, field-dependent magnetization measurements show the presence of multiple magnetic phase transitions at all temperatures below the ordering temperature down to T = 2 K, as shown in Figure 4(b). Resolving the nature of these phase transitions is complicated by the fact that by analogy to V-based lacunar spinels, it is likely that the magnetic phase diagram of GaMo₄Se₈ depends strongly on the direction at which

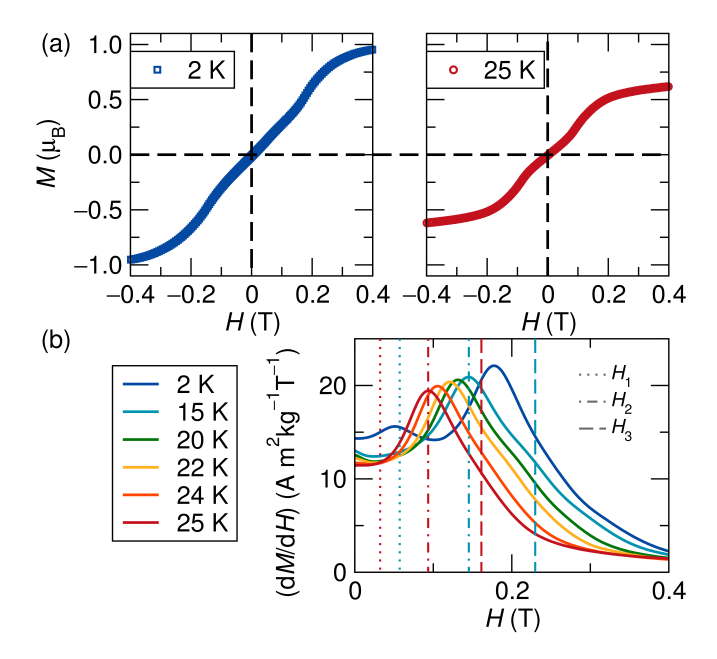


FIG. 4. (a) The saturation magnetization is around $1\,\mu_B/{\rm Mo_4}$ cluster, in agreement with DFT and molecular orbital theory. Multiple magnetic phase transitions are evident in field-dependent magnetization measurements. (b) Phase transitions are shown more clearly in the derivative of magnetization with respect to field. These transitions persist down to $T=2\,{\rm K}$, the lowest temperature measured.

the magnetic field is oriented relative to the polar axis of the crystal. As all of our data is collected using a powder sample under uniaxial applied magnetic field, different grains can have different magnetic phases, complicating the interpretation of bulk magnetization data. Nonetheless, by combining a variety of experimental and computational signatures of magnetic phase stability, we are able to understand the observed magnetic phase transitions and confirm the existence of a skyrmion phase.

A recently presented experimental technique for resolving magnetic phase diagrams is magnetoentropic mapping. This technique [31], relies on the Maxwell relation that $(\partial M/\partial T)_H = (\partial S/\partial H)_T$ to identify field driven magnetic phase transitions that are associated with a change in magnetic entropy. In particular, skyrmions form as a high entropy phase, so that the formation of skyrmions is typically associated with a positive entropy anomaly [31, 33, 34]. On a map of $(\partial S/\partial H)_T$, shown in Figure 5(b) we can see a red positive entropy anomaly that starts near the Curie temperature and broadens upon cooling. Overlaying this data with peaks in DC susceptibilities $(\partial M/\partial T)$, shown in Supplementary Figure S1, and $(\partial M/\partial H)$ vs. H curves, shown in Figure 4(b), as well as AC susceptibility measurements, shown in Supplementary Figure S2, we observe these signatures are in agreement with the transitions from the entropy map. From these measurements we can generate the phase diagram shown in Figure 5(a) which suggests that the high-entropy region corresponds

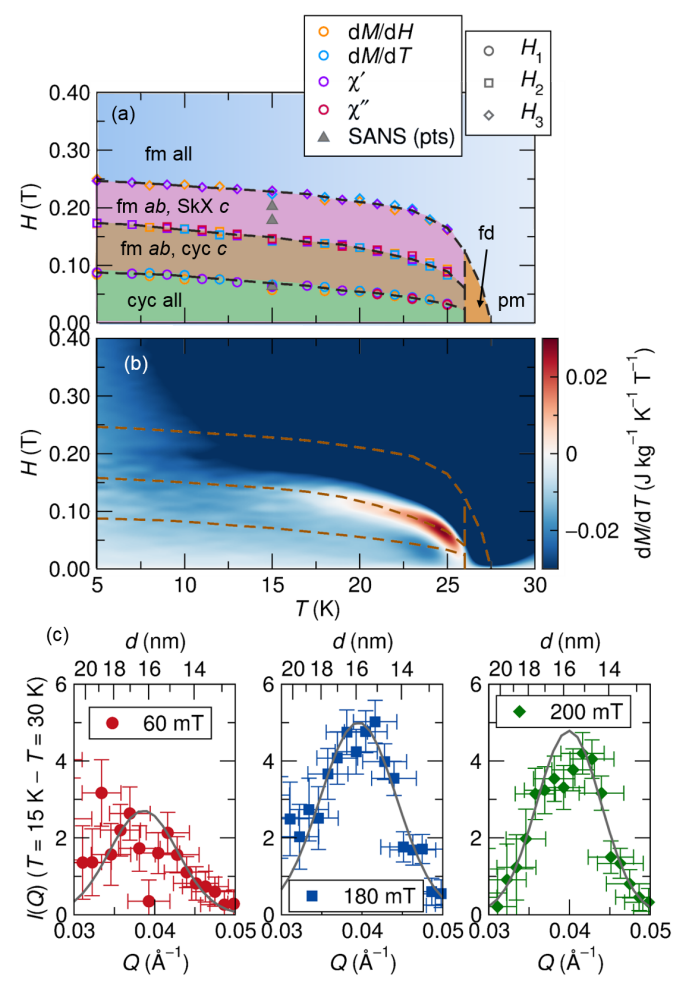


FIG. 5. (a) Using multiple bulk magnetization measurement techniques, we suggest a field vs. temperature phase diagram for GaMo₄Se₈. Based on theoretical calculations and the phase diagrams for the related V-compounds, we posit that the low field transition is a transition from cycloidal into ferromagnetic ordering in grains (denoted ab) where the field is mostly perpendicular to the polar axis. Upon increasing field, grains (denoted c) where the field is mostly aligned with the polar axis transition into a skyrmion phase and then become field polarized. Near the Curie temperature there is a fluctuation-disordered phase. (b) The transition into the proposed skyrmion phase in c-oriented grains is associated with an increase in magnetic entropy, shown as a red feature near the Curie temperature that broadens upon cooling. (c) SANS data shows the presence of approximately 16 nm magnetic periodicity at multiple applied fields at T = 15 K. The red points are in the cycloidal phase and the blue and green are in the skyrmion phase. The gray lines are Gaussian fits to guide the eye.

to a skyrmion phase with behavior similar to that seen in GaV_4Se_8 .

Susceptibility data reveals two additional transitions not visible in the magnetoentropic map, indicating the presence of phase transitions not associated with a large change in magnetic entropy. To unambiguously resolve these phase transitions, as well as to disentangle the con-

	A	D_{xy}	D_{yx}	K_u
	(10^{-13} J/m)	(10^{-4} J/m^2)		(10^4 J/m^3)
R3m	3.48	-2.35	2.35	7.34
Imm2	4.15	-5.00	-0.682	-182

TABLE I. Effective micromagnetic interaction parameters in the low-temperature limit for the R3m and Imm2 phases of $GaMo_4Se_8$.

tributions of the R3m and Imm2 phases in the powder, we turn to computational modeling. Our computational analysis relies on a magnetic cluster expansion Hamiltonian parameterized using density functional theory (DFT), which has been recently demonstrated to yield reliable magnetic phase diagrams for the lacunar spinels [14]. We are thus able to independently resolve the anisotropic magnetic phase diagrams expected in the R3m and Imm2 phases and rationalize the observed magnetic behavior of the biphasic powder.

First, we demonstrate that the zero-field, lowtemperature ground state magnetic configuration of the R3m phase is a cycloid with a predicted wavelength of 18 nm, while the Imm2 phase is a uniaxial ferromagnet. Figure 6(a) maps out the energy of the ferromagnetic state in both phases relative to the energy of the ground state magnetic phase. The Imm2 phase strongly favors magnetization along the b-axis, parallel to the shortest Mo-Mo bond. The R3m phase exhibits a predominantly easy-plane anisotropy, normal to the compressive distortion of the Mo₄ tetrahedron, with a threefold modulation favoring spin orientation towards the corners of the tetrahedron. While the Dzyaloshinskii-Moriya interaction (DMI) in the two phases is comparable in magnitude and favors cycloidal spin textures in the (ab)-planes [35], the large magnetocrystalline anisotropy of the Imm2 phase suppresses any spin configuration deviating from the b-axis, forcing a ferromagnetic ground state. In the R3m phase, the DMI overcomes the anisotropy energy and leads to the formation of equilibrium spin cycloids at the low energy wavevectors shown in Figure 6(b). The cycloids can form in any direction in the (ab)-plane, which is the plane perpendicular to the polar (c) axis of the R3m structure.

The low–temperature magnetic behavior of the R3m and Imm2 phases can be summarized using a conventional micromagnetic free energy density functional, which is directly comparable to that of other skyrmionhost materials[8, 36]:

$$E = A \sum_{ij} m_{i,j}^2 + \sum_{ijkn} D_{kn} \varepsilon_{ijk} m_i m_{j,n} + K_u m_u^2$$

where m is a magnetization unit vector, A is the exchange stiffness, D_{kn} is the Dzyaloshinkii coupling, and K_u is the uniaxial anisotropy constant defined with respect to the c-axis of the R3m phase, and the b-axis of the Imm2 phase. The micromagnetic parameters and

employed here are given in Table I. Having established the low-temperature, zero-field magnetic behavior of the two phases comprising our GaMo₄Se₈ sample, we proceed to construct the full field vs. temperature phase diagram of the material. We focus on the R3m phase, as shown in Figure 6(c), because the Imm2 phase remains a uniaxial ferromagnet at all fields within our experimental range and does not contribute to the observed phase transitions. For fields oriented along the (ab)-plane, the phase diagram is defined by a transition from the cycloidal ground state to a field-polarized ferromagnetic state near $H = 0.1 \,\mathrm{T}$. Below $\approx T_C/3$, this phase transition is first order, while at higher temperatures it proceeds as a second order transition through a canted cycloid intermediate. When the field is oriented along the c-axis, the low-field cycloid undergoes a first-order transition into a skyrmion lattice phase at around $H = 0.3 \,\mathrm{T}$, which appears to remain stable to very high fields, up to $H = 1.7 \,\mathrm{T}$. Magnetic order persists up to $T_C = 32 \,\mathrm{K}$, with a fluctuation-disordered Brazovskii region appearing immediately above T_C . While some quantitative discrepancies exist between this computational phase diagram and the experimental data, in particular in the range of fields for which skyrmions appear to be stable, the overall trends in phase behavior are informative for determining which phase transitions are being observed in our powder data.

The trends in phase behavior observed in the computational model confirm that the high–entropy region observed in the magnetoentropic map likely corresponds to a skyrmion phase in R3m grains with the c-axis nearly parallel to the applied field. Furthermore, we propose that the low field transition seen in the susceptibility data is from a cycloidal to a ferromagnetic state in R3m grains where the magnetic field is mostly aligned perpendicular to the polar axis. The high field transition is most likely a transition from the skyrmion lattice to a ferromagnetic state in R3m grains in which the magnetic field is mostly aligned along the polar (c) axis. Finally, the Imm2 phase contributes a ferromagnetic background, with no additional magnetic phase transitions.

To verify the presence of long–wavelength magnetic order in $GaMo_4Se_8$, we performed powder SANS measurements at 15 K in the regions we predict to correspond to cycloid and skyrmion stability. The points at which SANS data was taken are indicated on our proposed phase diagram in Figure 5(a) with triangle. Due to the small moment of $1\,\mu_B/Mo_4$ cluster and different grains in different magnetic phases, the signal is quite low. Nonetheless, after subtracting background data taken at $T=30\,\mathrm{K}$ (above the Curie temperature), we see one to two peaks in the SANS signal at all applied fields, shown in Figure 5(b), corresponding to a real-space magnetic periodicity of around 16 nm, in acceptable agreement with our theoretical calculations for cycloid/skyrmion periodicity (18 nm).

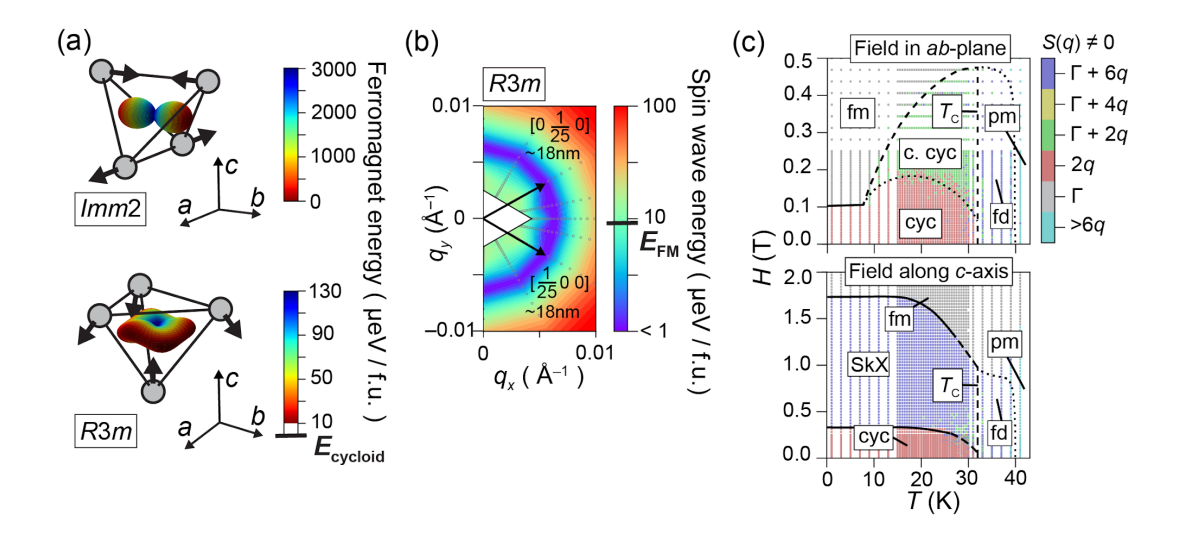


FIG. 6. (a) Computed magnetocrystalline anisotropy in the Imm2 and R3m phases of $GaMo_4Se_8$. Grey circles denote Mo atoms, and black arrows illustrate the direction of the Jahn-Teller distortion required to form each phase. The plotted color and distance from the tetrahedron center denote the energy of a ferromagnetic spin configuration oriented along the corresponding crystallographic direction. (b) Energy of spin wave configurations in the (ab)-plane of the R3m phase as a function of their q-vector, revealing the family of cycloid ground states with a predicted wavelength of ≈ 18 nm. (c) Computed magnetic phase diagram of the R3m phase for fields oriented along the c-axis or the (ab)-plane. Color denotes the magnetic structure factor S(q), while phase boundaries are drawn to best capture discontinuities in structure factor, suscetibility, heat capacity, and magnetization. Phase labels correspond to cycloid (cyc), canted cycloid (c. cyc), skyrmion (skX), ferromagnet (fm), fluctuation disordered (fd), and paramagnet (pm) regions.

IV. DISCUSSION

We have established that GaMo₄Se₈ undergoes a complex structural phase transition due to a relatively flat energy landscape in which multiple low temperature space groups have similar energies, as well as a competition between phases favored thermodynamically and kinetically. While the GaV₄(S/Se)₈ compounds exhibit only the R3m structure at low temperature, GaMo₄Se₈ undergoes a structural transition from the high temperature $F\overline{4}3m$ phase into two coexisting polar space groups, rhombohedral R3m, which is the ground state, and orthorhombic Imm2, which is metastable. In the lacunar spinel family, GeV₄S₈ undergoes a Jahn-Teller distortion into an *Imm*2 structure, likely because it has one extra electron in the t_2 orbital relative to GaV₄S₈, stabilizing a different splitting of the t_2 orbital [37]. We speculate that in GaMo₄Se₈, the increased filling of the t_2 orbital relative to the Vcompounds, along with enhanced spin-orbit coupling, creates an energy landscape with the Imm2 and R3mstructures much closer in energy than in other members of the family.

The competition between the stable and metastable crystal structures of $GaMo_4Se_8$ could be used to tune the multiferroic properties of $GaMo_4Se_8$, for instance by straining the material in such a way to stabilize one of the crystal structures. Our computational studies shows that the slight differences between the Imm2 and R3m structures have a dramatic impact on the magnetic properties due to a large change in magnetocrystalline

anisotropy. Thus, any strain which alters the relative stability of the two phases will in turn have a strong impact on magnetic behavior. Specifically, stabilization of the Imm2 phase leads to uniaxial ferromagnetism, while favoring the R3m phase leads to long-wavelength magnetic order with a cycloidal ground state and Néel-type skyrmions. The strong emergent magnetostructural coupling in $GaMo_4Se_8$ provides a route towards the mechanical control of exotic magnetism.

It is worth noting that extra diffraction peaks similar to those of the Imm2 phase in $GaMo_4Se_8$ were also observed in the low temperature diffraction patterns of the sulfide equivalent, $GaMo_4S_8$ and attributed to coexistence of the cubic phase [11]. Thus, it is possible that $GaMo_4S_8$ could also have coexisting rhombohedral and orthorhombic low temperature structures, and exhibit similarly strong emergent magnetostructural coupling. Given the recent exciting magnetic discoveries in $GaMo_4S_8$ [16], the discovery of an Imm2 phase in $GaMo_4Se_8$ merits a re-examination of the crystal structure evolution of $GaMo_4S_8$ with synchrotron resolution.

Finally, we have shown that the R3m phase of ${\rm GaMo_4Se_8}$ has a magnetic phase diagram with long-wavelength magnetic phases stable over a wide temperature and field range. ${\rm GaMo_4Se_8}$ has a higher Curie temperature than the V-compounds or ${\rm GaMo_4Se_8}$ at $T_C=27.5\,{\rm K}$, with cycloids and Néel-type skyrmions stable down to the lowest temperatures measured $(T=2\,{\rm K})$. With a field applied along the polar axis, cycloids are stable from $H=0.15\,{\rm T}$

and skyrmions are stable up to $H = 0.25 \,\mathrm{T}$ at $T = 5 \,\mathrm{K}$. SANS data show a magnetic periodicity of around 16 nm, in good agreement with our computational analysis (18 nm). Overall, the qualitative form of the phase diagram is in good agreement between our experimental results, computational analysis, and previous reports in the literature for materials of similar symmetry[14, 38-40]. However, there are deviations from experiment in the exact range of fields for which skyrmions are stable. The discrepancy in the cycloid to skyrmion transition is of a similar magnitude to the error in the Curie temperature and cycloid to in-plane ferromagnet transition, and is most likely a result of errors in the underlying DFT representation of GaMo₄Se₈ magnetism, as well as deviations in the q-factor from our assumed value of 2. The much larger discrepancy in the upper bound on skyrmion stability versus applied field is more likely a result of stray fields, which we neglect in our simulations. Finally, while we do not observe the complexity in magnetic ordering vector reported in GaMo₄S₈ [16], this difference may be a consequence of the sensitivity of data we are able to obtain from a powder sample as compared to a single crystal.

V. CONCLUSION

The combined experimental and computational investigation of the low-temperature structural and magnetic phase behavior of the $GaMo_4Se_8$ lacunar spinel has been carried out. We show that this material undergoes a Jahn-Teller distortion at $T=51\,\mathrm{K}$ into two co-existing structures – a metastable Imm2 configuration and the ground state R3m phase. These two phases both order magnetically at $T_C=27.5\,\mathrm{K}$, but exhibit dramatically different magnetic behavior due to differences in their magnetocrystalline anisotropy. While the Imm2 phase

is found from computation to be a uniaxial ferromagnet, the R3m phase favors a 16 nm cycloid ground state, and a Néel–skyrmion lattice under applied field. We conclude that the coexistence of these two phases with dramatically different magnetic properties makes $\rm GaMo_4Se_8$ a promising material for realizing mechanical control over exotic magnetism, as small energy differences separating the Imm2 and R3m phases translate into a very large change in magnetic behavior.

ACKNOWLEDGMENTS

This research was supported by the National Science Foundation (NSF) under DMREF Award DMR-1729489. Partial support from the NSF Materials Research Science and Engineering Center (MRSEC) at UC Santa Barbara, DMR-1720256 (IRG0-2) is gratefully acknowledged (D. A. K. and A.V.dV.) Use of the Shared Experimental Facilities of the UCSB MRSEC (NSF DMR 1720256) is acknowledged. The UCSB MRSEC is a member of the NSF-supported Materials Research Facilities Network (www.mrfn.org). We also acknowledge support from the Center for Scientific Computing (NSF DMR-1720256 and NSF CNS-1725797), as well as the National Energy Research Scientific Computing Center, a DOE Office of Science User Facility supported by DOE DE-AC02-05CH11231. Use of the Advanced Photon Source at Argonne National Laboratory was supported by the U. S. Department of Energy, Office of Science, Office of Basic Energy Sciences, under Contract No. DE-AC02-06CH11357. We thank Dr. S. Lapidus of 11-BM at the Advanced Photon Source for helpful contributions. We acknowledge the support of Dr. M. Bleuel and the National Institute of Standards and Technology, U.S. Department of Commerce, in providing the neutron research facilities used in this work.

- [1] I. I. Mazin, H. O. Jeschke, K. Foyevtsova, R. Valenti, and D. I. Khomskii, Na₂IrO₃ as a Molecular Orbital Crystal, Phys. Rev. Lett. **109**, 197201 (2012).
- [2] Z. Hiroi, Structural Instability of the Rutile Compounds and its Relevance to the Metal–Insulator Transition of VO₂, Progr. Solid State Chem. 43, 47 (2015).
- [3] S. V. Streltsov and D. I. Khomskii, Covalent Bonds Against Magnetism in Transition Metal Compounds, Proc. Natl. Acad. Sci. 113, 10491 (2016).
- [4] E. C. Schueller, J. L. Zuo, J. D. Bocarsly, D. A. Kitchaev, S. D. Wilson, and R. Seshadri, Modeling the Structural Distortion and Magnetic Ground State of the Polar Lacunar Spinel GaV₄Se₈, Phys. Rev. B 100, 045131 (2019).
- [5] H.-S. Kim, J. Im, M. J. Han, and H. Jin, Spin-Orbital Entangled Molecular j_{eff} States in Lacunar Spinel Compounds, Nat. Commun. 5, 3988 (2014).
- [6] Y. Fujima, N. Abe, Y. Tokunaga, and T. Arima, Thermodynamically Stable Skyrmion Lattice at Low Temperatures in a Bulk Crystal of Lacunar Spinel GaV₄Se₈, Phys. Rev. B

- 95, 180410 (2017).
- [7] E. Ruff, A. Butykai, K. Geirhos, S. Widmann, V. Tsurkan, E. Stefanet, I. Kezsmarki, A. Loidl, and P. Lunkenheimer, Polar and Magnetic Order in GaV₄Se₈, Phys. Rev. B 96, 165119 (2017).
- [8] S. Bordacs, A. Butykai, B. G. Szigeti, J. S. White, R. Cubitt, A. O. Leonov, S. Widmann, D. Ehlers, H.-A. K. von Nidda, V. Tsurkan, A. Loidl, and I. Kezsmarki, Equilibrium Skyrmion Lattice Ground State in a Polar Easy-plane Magnet, Sci. Rep. 7, 7584 (2017).
- [9] R. Pocha, D. Johrendt, and R. Pottgen, Electronic and Structural Instabilities in GaV₄S₈ and GaMo₄S₈, Chem. Mater. 12, 2882 (2000).
- [10] M. Francois, O. V. Alexandrov, K. Yvon, H. B. Yaich-Aerrache, P. Gougeon, M. Potel, and M. Sergent, Structural Phase Transition in GaMo₄Se₈ and AlMo₄Se₈ by X-ray Powder Diffraction, Z. Kristallogr. Cryst. Mater. 200, 47 (1992).

- [11] M. Francois, W. Lengauer, and K. Yvon, Structural Phase Transition in GaMo₄S₈ by X-ray Powder Diffraction, Z. Kristallogr. Cryst. Mater. 196, 111 (1990).
- [12] A. K. Rastogi, A. Berton, J. Chaussy, R. Tournier, M. Potel, R. Chevrel, and M. Sergent, Itinerant Electron Magnetism in the Mo₄ Tetrahedral Cluster Compounds GaMo₄S₈, GaMo₄Se₈, and GaMo₄Se₄Te₄, J. Low Temp. Phys. **52**, 539 (1983).
- [13] A. K. Rastogi and E. P. Wohlfarth, Magnetic Field-Induced Transitions in the Mo₄ Cluster Compounds GaMo₄S₈ and GaMo₄Se₈ Showing Heavy Fermion Behaviour, Phys. Stat. Sol. (b) 142, 569 (1987).
- [14] D. A. Kitchaev, E. C. Schueller, and A. Van der Ven, Mapping Skyrmion Stability in Uniaxial Lacunar Spinel Magnets from First-Principles, Phys. Rev. B 101, 054409 (2020).
- [15] M. Y. Jeong, S. H. Chang, B. H. Kim, J.-H. Sim, A. Said, D. Casa, T. Gog, E. Janod, L. Cario, S. Yunoki, M. J. Han, and J. Kim, Direct Experimental Observation of the Molecular $J_{eff}=3/2$ Ground State in the Lacunar Spinel GaTa $_4$ Se $_8$, Nat. Commun. **8**, 782 (2017).
- [16] A. Butykai, D. Szaller, L. F. Kiss, L. Balogh, M. Garst, L. DeBeer-Schmitt, T. Waki, Y. Tabata, H. Nakamura, I. Kezsmarki, and S. Bordacs, Squeezing Magnetic Modulations by Enhanced Spin-Orbit Coupling of 4d Electrons in the Polar Semiconductor GaMo₄S₈, arXiv 1910.11523 (2019).
- [17] G. Kresse and J. Furthmuller, Efficient Iterative Schemes for Ab Initio Total-Energy Calculations Using a Plane-Wave Basis Set, Phys. Rev. B 54, 11169 (1996).
- [18] P. E. Bloch, Projector Augmented-Wave Method, Phys. Rev. B 50, 17953 (1994).
- [19] G. Kresse and D. Joubert, From Ultrasoft Pseudopotentials to the Projector Augmented-Wave Method, Phys. Rev. B 59, 1758 (1999).
- [20] J. P. Perdew, K. Burke, and M. Ernzerhof, Generalized Gradient Approximation Made Simple, Phys. Rev. Lett. 77, 3865 (1996).
- [21] B. J. Campbell, H. T. Stokes, D. E. Tanner, and D. M. Hatch, ISODISPLACE: a web-based tool for exploring structural distortions, J. Appl. Cryst. 39, 607 (2006).
- [22] S. P. Ong, W. D. Richards, A. Jain, G. Hautier, M. Kocher, S. Cholia, D. Gunter, V. L. Chevrier, K. A. Persson, and G. Ceder, Python Materials Genomics (pymatgen): A Robust, Open-Source Python Library for Materials Analysis, Comput. Mater. Sci. 68, 314 (2013).
- [23] R. Drautz and M. Fähnle, Spin-Cluster Expansion: Parametrization of the General Adiabatic Magnetic Energy Surface with ab initio Accuracy, Phys. Rev. B 69, 104404 (2004).
- [24] J. C. Thomas and A. Van der Ven, The Exploration of Nonlinear Elasticity and its Efficient Parameterization for Crystalline Materials, J. Mech. Phys. Solids 107, 76 (2017).
- [25] A. Van der Ven, J. C. Thomas, B. Puchala, and A. R. Natarajan, First-Principles Statistical Mechanics of Multicomponent Crystals, Annu. Rev. Mater. Res. 48, 27

- (2018).
- [26] A. Van de Walle and G. Ceder, Automating First-Principles Phase Diagram Calculations, J. Phase Equilib. 23, 348 (2002).
- [27] S. Jakob, Strukturen, Magnetismus und Phasenumwandlungen der Mott-Isolatoren $Ga(M_{4-x}M'_x)Q_8$ und $(M_{4-x}M'_x)Q_4I_4(M, M' = Mo, Nb, Ta; Q = S, Se; <math>x = 0$ –4), Ph.D. thesis, Ludwig-Maximilians-Universitat Munchen (2010).
- [28] A. A. Coelho, TOPAS and TOPAS-Academic: An Optimization Program Integrating Computer Algebra and Crystallographic Objects Written in C++, J. Appl. Crystallogr. 51, 210 (2018).
- [29] K. Momma and F. Izumi, VESTA3 for Three-Dimensional Visualization of Crystal, Volumetric and Morphology Data, J. Appl. Crystallogr. 44, 1272 (2011).
- [30] S. R. Kline, Reduction and Analysis of SANS and USANS Data Using IGOR Pro, J. Appl. Cryst. 39, 895 (2006).
- [31] J. D. Bocarsly, R. F. Need, R. Seshadri, and S. D. Wilson, Magnetoentropic Signatures of Skyrmionic Phase Behavior in FeGe, Phys. Rev. B 97, 100404 (2018).
- [32] M. C. Kemei, P. T. Barton, S. L. Moffitt, M. W. Gaultois, J. A. Kurzman, R. Seshadri, M. R. Suchomel, and Y.-I. Kim, Crystal Structures of Spin-Jahn-Teller-Ordered MgCr₂O₄ and ZnCr₂O₄, J. Phys.: Condens. Matter 25, 326001 (2013).
- [33] J. D. Bocarsly, C. Heikes, C. M. Brown, S. D. Wilson, and R. Seshadri, Deciphering Structural and Magnetic Disorder in the Chiral Skyrmion Host Materials $\text{Co}_x\text{Zn}_y\text{Mn}_z$ (x+y+z=20), Phys. Rev. Materials **3**, 014402 (2019).
- [34] L. Kautzsch, J. D. Bocarsly, C. Felser, S. D. Wilson, and R. Seshadri, Controlling Dzyaloshinskii-Moriya Interactions in the Skyrmion Host Candidates $FePd_{1-x}Pt_xMo_3N$, Phys. Rev. Materials **4**, 024412 (2020).
- [35] D. A. Kitchaev, I. J. Beyerlein, and A. Van der Ven, Phenomenology of Chiral Dzyaloshinskii-Moriya Interactions in Strained Materials, Phys. Rev. B 98, 214414 (2018).
- [36] R. Takagi, D. Morikawa, K. Karube, N. Kanazawa, K. Shibata, G. Tatara, Y. Tokunaga, T. Arima, Y. Taguchi, Y. Tokura, and S. Seki, Spin-Wave Spectroscopy of the Dzyaloshinskii-Moriya Interaction in Room-Temperature Chiral Magnets Hosting Skyrmions, Phys. Rev. B 95, 220406 (2017).
- [37] D. Bichler, V. Zinth, D. Johrendt, O. Heyer, M. K. Forthaus, T. Lorenz, and M. M. Abd-Elmeguid, Structural and Magnetic Phase Transitions of the V₄-cluster compound GeV₄S₈, Phys. Rev. B 77, 212102 (2008).
- [38] A. Bogdanov and A. Hubert, Thermodynamically Stable Magnetic Vortex States in Magnetic Crystals, J. Magn. Magn. Mater. 138, 255 (1994).
- [39] U. Güngördü, R. Nepal, O. A. Tretiakov, K. Belashchenko, and A. A. Kovalev, Stability of Skyrmion Lattices and Symmetries of Quasi-Two-Dimensional Chiral Magnets, Phys. Rev. B 93, 064428 (2016).
- [40] J. Rowland, S. Banerjee, and M. Randeria, Skyrmions in Chiral Magnets with Rashba and Dresselhaus Spin-Orbit Coupling, Phys. Rev. B **93**, 020404 (2016).